Supplemental Material for: Graphene allotropes under extreme uniaxial strain: An ab-initio theoretical study.

Zacharias G. Fthenakis
Physics and Astronomy Department, Michigan State University, East Lansing, Michigan 48824, USA and Institute of Electronic Structure and Laser, FORTH, P.O. Box 1527, 71110 Heraklio, Crete, Greece

Nektarios N. Lathiotakis
Theoretical and Physical Chemistry Institute, National Hellenic Research Foundation, Vass. Constantinou 48, GR-11635 Athens, Greece and Max-Planck-Institut für Mikrostrukturphysik, Weinberg 2, D-06120 Halle (Saale), Germany

(Dated: April 21, 2015)

Main manuscript abstract: Using density functional theory calculations, we study the response of three representative graphene allotropes (two Pentaheptites and Octagraphene) as well as graphene, to uniaxial strain up to their fracture limit. Those allotropes can be seen as distorted graphene structures formed upon periodically arranged Stone - Walles transformations. We calculate their mechanical properties (Young's modulus, Poison's ratio, speed of sound, ultimate tensile strength and the corresponding strain), and we describe the pathways of their fracture. Finally, we study strain as a factor for the conversion of graphene into those allotropes upon Stone - Walles transformations. For specific sets of Stone - Walles transformations leading to an allotrope, we determine the strain directions and the corresponding minimum strain value, for which the allotrope is more favorable energetically than graphene. We find that the minimum strain values which favor those conversions are of the order of 9-13%. Moreover, we find that the energy barriers for the Stone - Walles transformations, decrease dramatically under strain, however, they remain prohibitive for structural transitions. Thus, strain alone can not provide a synthetic route to these allotropes, but could be a part of composite procedures for this purpose.

Supplemental Information summary: We present all details of the fits to polynomial functions of stress strain plots in order to estimate the Young's moduli and Poisson's ratios of the structures under study in different directions described in the main manuscript. We also show that the relation between σ/ε versus ε up to the UTS is not linear. Moreover, we use a simple model to estimate the k value ($k = Ev/2$) for OcGr as a function of the strain direction for the two different sets of SWTs of our study leading to OcGr.

A. Fitting details

As mentioned in the main manuscript, to estimate the Poisson's ratio ν and Young's modulus E at ambient strain for each structure and strain direction of our study, we use the least square fitting method to fit the (ε, $\varepsilon_\perp$) points to a quadratic fitting function of the form

$$\varepsilon_\perp = \nu_1 \varepsilon^2 - \nu\varepsilon \tag{S1}$$

and (ε, σ) points to a 3rd degree polynomial of the form

$$\sigma = F\varepsilon^3 + D\varepsilon^2 + E\varepsilon, \tag{S2}$$

for ε values in the range [-0.1, 0.1].

The form of Eq. S1 seems to be adequate to describe quite accurately the relations between ε and $\varepsilon_\perp$ for the structures of our study, as shown in Fig. 2(b) of the main manuscript and Fig. S1(b). A sole exception is the OcGr case for strain along e_{se} direction, since as it is clearly shown in Fig. 2(b) of the main manuscript, that the relation between ε and $\nu = -\varepsilon_\perp/\varepsilon$ is by no means linear. In that particular case, we adopt a fitting function of the form

$$\varepsilon_\perp = \nu_2 \varepsilon^3 + \nu_1 \varepsilon^2 - \nu\varepsilon, \tag{S3}$$

which seems to be appropriate for that fit. The values of ν_1 and ν, as well as the correlation coefficient R^2 for the fits are included presented in Tab. S1.

The fitting functions of the form of Eq. S2 are shown in Fig. S1(a). The F, D and E values for each fit are presented in Table S1. Just for comparison we also fitted the (ε, σ) points to the same fitting function, as well as the (ε, σ/ε) points to the function

$$\sigma/\varepsilon = F\varepsilon^2 + D\varepsilon + E \tag{S4}$$

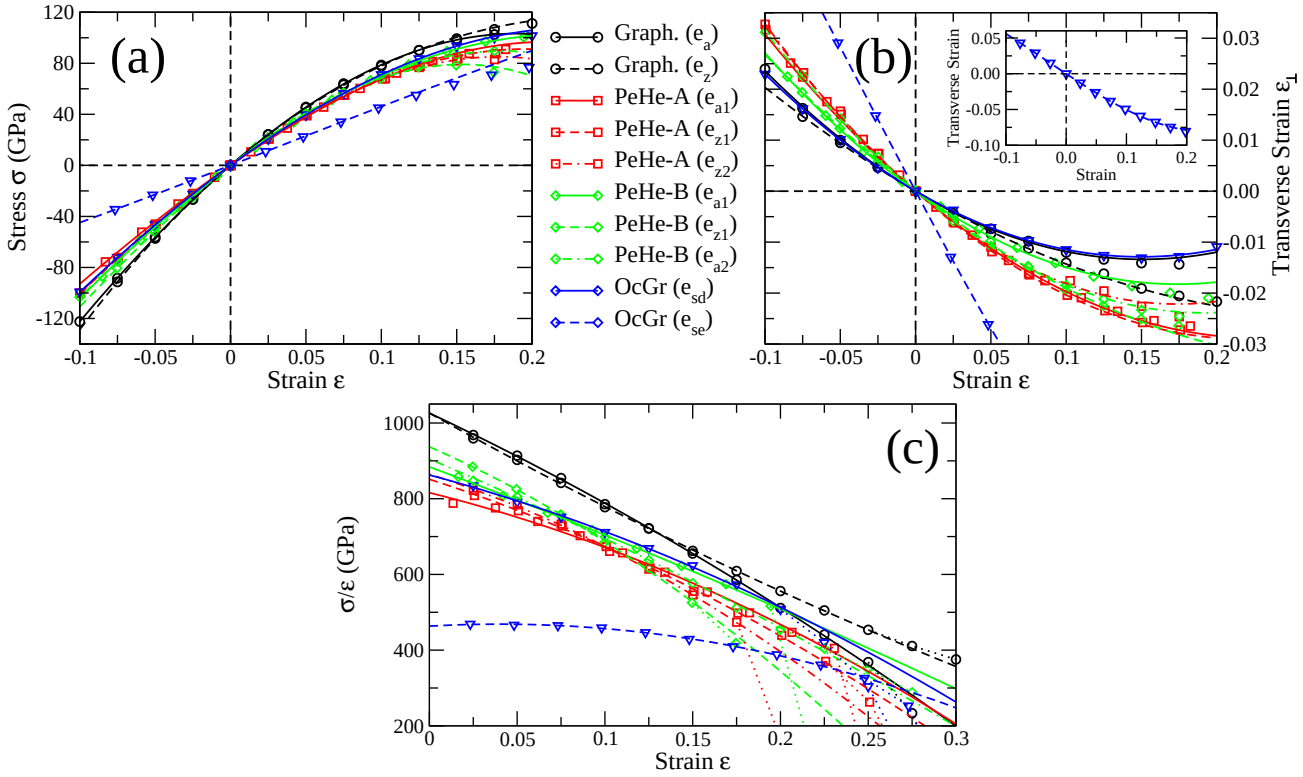

FIG. S1: Fits to estimate (a) Young's modulus E and (b) Poisson's ratio ν. Lines present the fitting functions according to Eqs. S1 and S2 for the strain range [-0.1, 0.1], except in (b) for the OcGr strained along e_{se} direction, where Eq. S3 has been used for the fit, for the same range of ε. In (c) we show σ/ε as a function of strain ε. If $\sigma = E\varepsilon + D\varepsilon^2$, then the curves in (c) should be straight lines. The curves in (c) correspond to fittings according to Eq. S4.

Structure	direction	ν_1	ν	R^2	F (GPa)	D (GPa)	E (GPa)	R^2
Graphene	e_a	0.586998	0.177222	0.9996	-1834.400	-2180.762	1024.126	0.999987
	e_z	0.302497	0.173224	0.9994	1351.574	-2537.734	1020.176	0.999986
PeHe-A	e_{a1}	0.552949	0.252569	0.9994	-2203.236	-1270.180	824.913	0.99998
	e_{z1}	0.598259	0.263706	0.9996	-1835.280	-1652.989	859.660	0.999987
	e_{z2}	0.734046	0.255031	0.998	-2956.128	-1646.310	864.900	0.99994
PeHe-B	e_{a1}	0.605278	0.210213	0.9996	-791.424	-1710.944	882.192	0.999997
	e_{z1}	0.388375	0.228903	0.9995	-4062.802	-2123.779	937.140	0.999994
	e_{a2}	0.649711	0.249098	0.99993	-3086.814	-1662.229	897.075	0.999996
OcGr	e_{sd}	0.574898	0.172129	0.99994	-1362.764	-1408.787	865.533	0.999998
	e_{se}	~~0.267039~~	~~0.538316~~	~~0.9997~~	-573.363	60.915	460.562	0.99996

TABLE S1: Fitted parameters for the estimation of Poisson's ratios and Young's moduli, for $-0.1 \leq \varepsilon \leq 0.1$, according to Eqs. S1 and S2. Especially for OcGr strained along e_{se} direction, a more appropriate fitting function, namely $\varepsilon_\perp = 2.720500\varepsilon^3 + 0.276210\varepsilon^2 - 0.558299\varepsilon$, ($R^2 = 0.99998$) was adopted for Poisson's ratio estimation. The strike-through lines denote that the particular fit was not used to evaluate the Poisson's ratio.

for $\varepsilon > 0$ values up to the strain corresponding to the ultimate tensile stress (UTS) for each case. Obviously, for the fitting of Eq. S4, the (ε σ)=(0,0) point was not included. The F, D and E values of those fits, as well as the corresponding correlation coefficient R^2 are presented in Tables S2 and S3.

It is worth noting that both Eqs. S2 and S1 (and Eq. S3 for OcGr strained along e_{se} direction) are quite accurate in describing the σ and $\varepsilon_\perp$ behavior versus ε, even for strain values in the range $0.1 > \varepsilon > 0.2$, which have not been taken in account for the fit and typically do not exceed the UTS limit. This is clearly shown in Fig. S1.

As we see, the obtained values for the Young moduli are not very sensitive on the details of fit performed. Thus,

Structure	direction	F (GPa)	D (GPa)	E (GPa)	R^2	ε range
Graphene	e_a	-1223.041	-2346.303	1034.012	0.999995	$0 \leq \varepsilon \leq 0.175$
	e_z	1533.663	-2690.550	1032.681	0.999996	$0 \leq \varepsilon \leq 0.225$
PeHe-A	e_{a1}	-455.795	-1910.023	866.091	0.99991	$0 \leq \varepsilon \leq 0.275$
	e_{z1}	-1613.250	-1836.176	871.661	0.99998	$0 \leq \varepsilon \leq 0.200$
	e_{z2}	-3871.357	-1583.781	869.975	0.99998	$0 \leq \varepsilon \leq 0.175$
PeHe-B	e_{a1}	-1769.632	-1463.420	869.165	0.999988	$0 \leq \varepsilon \leq 0.200$
	e_{z1}	-6061.944	-1742.350	923.392	0.99995	$0 \leq \varepsilon \leq 0.150$
	e_{a2}	658.994	-2552.033	942.539	0.99994	$0 \leq \varepsilon \leq 0.225$
OcGr	e_{sd}	-4034.183	-836.612	838.792	0.99997	$0 \leq \varepsilon \leq 0.200$
	e_{se}	-3367.557	294.025	461.021	0.999987	$0 \leq \varepsilon \leq 0.250$

TABLE S2: Fitting stress - strain curve parameters using Eq. S2 for ε in the range shown in the last column.

Structure	direction	F (GPa)	D (GPa)	E (GPa)	R^2	ε range
Graphene	e_a	-1880.786	-2192.014	1026.142	0.99975	$0 < \varepsilon \leq 0.175$
	e_z	1192.860	-2589.717	1026.230	0.99983	$0 < \varepsilon \leq 0.225$
PeHe-A	e_{a1}	-2957.127	-1148.711	815.756	0.997	$0 < \varepsilon \leq 0.275$
	e_{z1}	-2898.357	-1489.601	851.206	0.9992	$0 < \varepsilon \leq 0.200$
	e_{z2}	-4348.858	-1473.603	864.511	0.9992	$0 < \varepsilon \leq 0.175$
PeHe-B	e_{a1}	-764.576	-1724.826	883.997	0.9995	$0 < \varepsilon \leq 0.200$
	e_{z1}	-4611.246	-2041.640	937.008	0.9991	$0 < \varepsilon \leq 0.150$
	e_{a2}	-1257.691	-1977.044	904.855	0.9985	$0 < \varepsilon \leq 0.225$
OcGr	e_{sd}	-2521.152	-1242.989	862.672	0.9987	$0 < \varepsilon \leq 0.200$
	e_{se}	-3270.161	261.828	463.353	0.9991	$0 < \varepsilon \leq 0.250$

TABLE S3: Fitting stress - strain curve parameters using Eq. S4 for ε in the range shown in the last column.

the error of our fitting procedure, estimated as the range of the obtained values for different fits, is less than 2% and only in in two cases, PeHe-A in e_{a1}, and PeHe-B in e_{a2} it rises to 6% and 5%, respectively.

On the contrary, the obtained values of D and, especially, F are very sensitive on the fitting procedure. However, the values of Tables S2 and S3 are expected to be relatively more reasonable since the non-linear terms become more important for large strain. Thus, with an expected error that can be of the order of 10-40%, we can only give rough estimates of D as the average of the values in Tables S2 and S3. For graphene, we obtain $D \sim -2.3 \times 10^3$ GPa, $\sim -2.6 \times 10^3$ GPa, for e_a, e_z, respectively. For PeHe-A, we obtain $D \sim -1.5 \times 10^3$ GPa, $\sim -1.7 \times 10^3$ GPa, and $\sim -1.5 \times 10^3$ GPa for the directions e_{a1}, e_{z1}, e_{z2}, respectively. For PeHe-B, $D \sim -1.6 \times 10^3$ GPa, $\sim -1.9 \times 10^3$ GPa, $\sim -2.3 \times 10^3$ GPa, for e_{a1}, e_{z1}, e_{a2}, respectively. Finally, for OcGr, we get $D \sim -1.0 \times 10^3$ GPa, and $\sim 0.28 \times 10^3$ GPa for the e_{sd} and e_{se} directions.

B. k for Octagraphene

In order to estimate the strain directions that favours the conversion of graphene, PeHe-A and PeHe-B to OcGr we need to know the parameter $k = k_O = Ev/2$ of OcGr. k_O can not be assumed independent on the strain direction unlike PeHe-A and PeHe-B, since OcGr is highly anisotropic in terms of Young's modulus E. Therefore, k_O depends on the strain direction defined by the strain angle ϕ. Moreover, since the final OcGr structure has different orientations, which depend on the conversion pathways, $k_O(\phi)$ should be different for the conversion paths $G \overset{A}{\rightarrow} O$ and $G \overset{B}{\rightarrow} O$.

Due to symmetry reasons arising from the square symmetry of the OcGr lattice, $k_O(\phi) = k_O(\pi/2 - \phi) = k_O(-\phi) = k_O(\pi - \phi) = k_O(\pi/2 + \phi)$. Consequently, we only need to know the dependence of k_O for $0 \leq \phi \leq \pi/4$. Just for convenience we assume that $k_O(\phi) = (k_O(\pi/4) - k_O(0)) \tan\phi + k_O(0)$, for $\phi \in [0, \pi/4]$, which is an almost linear relation between k_O and ϕ. Due to the relation $k_O(\phi) = k_O(\pi/2 - \phi)$, for $\phi \in [0, \pi/4]$, $k_O(\pi/2 - \phi) =$

$(k_O(\pi/4) - k_O(0)) \tan\phi + k_O(0)$. For $\theta = \pi/2 - \phi$, we find

$$\begin{aligned} k_O(\theta) &= (k_O(\pi/4) - k_O(0)) \tan(\pi/2 - \theta) + k_O(0) \\ &= (k_O(\pi/4) - k_O(0)) \cot(\theta) + k_O(0), \end{aligned} \tag{S5}$$

where $\pi/4 \leq \theta \leq \pi/2$. The above relations in combination with the relation $k_O(\phi) = k_O(-\phi)$ for negative angles, yield

$$k_O(\phi) = \begin{cases} (k_O(\pi/4) - k_O(0)) \tan|\phi| + k_O(0), & \text{for } |\phi| \leq \pi/4 \\ (k_O(\pi/4) - k_O(0)) \cot|\phi| + k_O(0), & \text{for } \pi/4 \leq |\phi| \leq \pi/2. \end{cases} \tag{S6}$$

For the $G \xrightarrow{A} O$ conversion path, $k_O(\phi = 0) = k_O(e_{se})$, $k_O(\phi = \pi/4) = k_O(e_{sd})$, where $k_O(e_{se})$ and $k_O(e_{sd})$ are the k values of OcGr for the strain directions e_{se} and e_{sd}, respectively. For a strain direction defined in fractional coordinates as (n,m), $\tan\phi = a_{O,y}/a_{O,x} = m/(2n)$. Thus,

$$k_O(n,m) = \begin{cases} (k_O(e_{sd}) - k_O(e_{se}))|m/(2n)| + k_O(e_{se}), & \text{for } |m| \leq |2n| \\ (k_O(e_{sd}) - k_O(e_{se}))|2n/m| + k_O(e_{se}), & \text{for } |m| \geq |2n|. \end{cases} \tag{S7}$$

In turn, for the $G \xrightarrow{B} O$ conversion path, $k_O(\phi = 0) = k_O(e_{sd})$, $k_O(\phi = \pi/4) = k_O(e_{se})$ and $\tan\phi = a_{O,y}/a_{O,x} = m/n$. Thus,

$$k_O(n,m) = \begin{cases} (k_O(e_{se}) - k_O(e_{sd}))|m/n| + k_O(e_{sd}), & \text{for } |m| \leq |n| \\ (k_O(e_{se}) - k_O(e_{sd}))|n/m| + k_O(e_{sd}), & \text{for } |m| \geq |n|. \end{cases} \tag{S8}$$

The values of $k_O(e_{se})$ and $k_O(e_{sd})$ are $k_O(e_{se}) \approx 14.2$ eV and $k_O(e_{sd}) \approx 26.7$ eV. In Fig. S2 we show k_O for OcGr as a function of the angle ϕ for both $G \xrightarrow{A} O$ and $G \xrightarrow{B} O$ conversion paths.

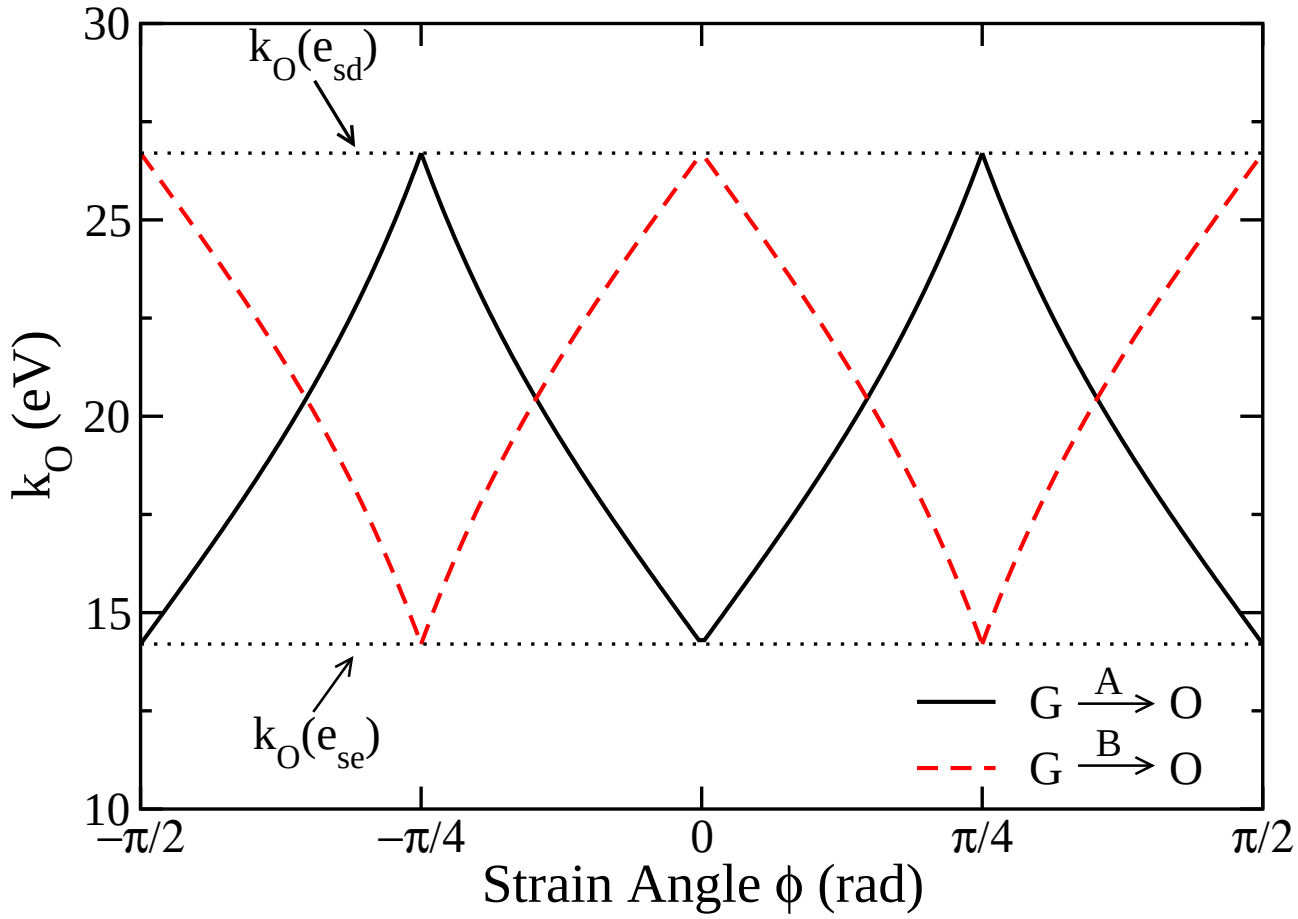

FIG. S2: k_O for OcGr as a function of the strain angle ϕ for $G \xrightarrow{A} O$ and $G \xrightarrow{B} O$ paths.